Edge states and local electronic structure around an adsorbed impurity in a topological superconductor

Yuan-Yen Tai,[1] Hongchul Choi,[1] Towfiq Ahmed,[1] C. S. Ting,[2] and Jian-Xin Zhu[1,3]

[1]*Theoretical Division, Los Alamos National Laboratory, Los Alamos, New Mexico 87545, USA*

[2]*Texas Center for Superconductivity and Department of Physics, University of Houston, Houston, Texas 77004, USA*

[3]*Center for Integrated Nanotechnologies, Los Alamos National Laboratory, Los Alamos, New Mexico 87545, USA*

Recently, topological superconducting states have attracted much interest. In this paper, we consider a topological superconductor with Z_2 topological mirror order [Y.-Y. Tai *et al.*, Phys. Rev. B **91**, 041111(R) (2015)] and $s_\pm$-wave superconducting pairing symmetry, within a two-orbital model originally designed for iron-based superconductivity [Y.-Y. Tai *et al.*, Europhys. Lett. **103**, 67001 (2013)]. We predict the existence of gapless edge states. We also study the local electronic structure around an adsorbed interstitial magnetic impurity in the system, and find the existence of low-energy in-gap bound states even with a weak spin polarization on the impurity. We also discuss the relevance of our results to a recent scanning tunneling microscopy experiment on a Fe(Te,Se) compound with an adsorbed Fe impurity [J.-X. Yin *et al.*, Nat. Phys. **11**, 543 (2015)], for which our density functional calculations show the Fe impurity is spin polarized.

I. INTRODUCTION

Topological superconductors (TSCs) have attracted much interest on their potential application to fault-tolerance quantum computation [1] and superconducting spintronics [2]. The TSC can be designed through the interface of a topological insulator with a fully gapped superconductor [3] or by engineering through the interface of a ferromagnetic-superconducting nanostructure under several special conditions [4–14]. Most of these efforts were aimed to look for the *edge states* and *in-gap bound states* in a fully gapped superconductor. There are two types of edge states for a two-dimensional (2D) TSC. The first type is a *chiral* edge state in a time-reversal-symmetry-broken superconducting pairing state such as $[p_x + ip_y]_{\uparrow\uparrow}$ [15,16]. The second type is a *helical* edge state in a time-reversal-symmetry-invariant pairing state such as $[p_x \pm ip_y]_{\uparrow\downarrow}$ [3,17]. Recently, the crystalline symmetry-protected topological phase with a mirror Chern number has been studied in a triplet pairing state of Sr_2RuO_4 [18], for which chiral edge states are obtained [16]. A realization of helical edge states can be established in a junction formed by an s-wave superconductor and a strong topological insulator (TI), mimicking a time-reversal-symmetry-preserved p-wave superconducting pairing state [3].

In this paper, we propose a feasible scenario to realize a helical topological mirror superconductor (HTMS) based on the coexistence of interaction-driven Z_2 topological mirror order and $s_\pm$-wave pairing symmetry. Our concept is based on the nature of a topological metal, where the superconductivity can be generated through a finite Fermi surface with electron (hole) Fermi pockets. The Z_2 mirror topological order creates robust edge states even in the presence of a fully gapped $s_\pm$-wave pairing symmetry. We further analyze the local electronic structure of an adsorbed interstitial magnetic impurity (IMI) in the 2D bulk of an HTMS, and identify the different consequences from topological and nontopological superconductors. It is important to note that, since the superconductivity is intrinsically inherited from the normal-state band structure, our proposal avoids the need to make a TI-SC heterostructure

for helical edge states. To show our model in a real-material context, we also carry out density functional theory (DFT) calculations for an adsorbed interstitial Fe impurity (IFI) in the recently discovered 11 family of iron-based superconductors FeSe, and find the adsorbed Fe atom to be spin polarized. Therefore, our results have a direct relevance to a recent scanning tunneling microscopy (STM) experiment on Fe(Te,Se) SCs, where a robust zero-energy bound state (ZBS) has been found around an adsorbed Fe atom [19].

II. MODEL SETUP

We consider the following effective Hamiltonian to describe the coexistence of Z_2 topological mirror order with $s_\pm$-pairing symmetry,

$$\mathcal{H}^{\text{TSC}} = \mathcal{T}[t_{1-6},\mu] + \mathcal{V}[\lambda_{\text{AOH}}] + \mathcal{P}[\Delta]. \qquad (1)$$

Here, $\mathcal{T}$ is the kinetic energy with optimized hopping terms (t_{1-6}) and chemical potential (μ) to describe the low-energy physics that was originally designed for a Fe-based compound [20,21], $\mathcal{V}$ is responsible for the emergent Z_2 topological mirror order [22] with tunable anomalous orbital Hall order (λ_{AOH}) for a d-wave form factor $\lambda_s(\mathbf{k}) = i(-1)^{\alpha s}\lambda_{\text{AOH}}[\cos(k_x) - \cos(k_y)]_{\alpha,\bar{\alpha}}$ (where $\alpha \in d_{xz},d_{yz}$, $s \in \uparrow\downarrow$), and $\mathcal{P}$ is the $s_\pm$-wave pairing order (Δ) with the form factor $\Delta(\mathbf{k}) = 4\Delta[\cos(k_x)\cos(k_y)]_{\uparrow\downarrow}$ in a 1-Fe Brillouin zone (BZ). Here, we write down the details of $\mathcal{H}^{\text{TSC}}$ in real-space formalism,

$$\mathcal{T} = \sum_{IJ,\alpha\beta,s} c^\dagger_{I\alpha s}\left(t^{\alpha\beta}_{IJ} - \mu\,\delta_{IJ}\delta_{\alpha\beta}\right)c_{J\beta s},$$

$$\mathcal{V} = \sum_{\langle IJ\rangle,\alpha,s} i(-1)^s \lambda_{\text{AOH}} \nu^{\alpha\bar{\alpha}}_{IJ} c^\dagger_{I\alpha s} c_{J\bar{\alpha}s}, \qquad (2)$$

$$\mathcal{P} = \sum_{IJ,\alpha,s} (\Delta c^\dagger_{I\alpha s} c^\dagger_{J\alpha s'} + \text{H.c.}),$$

were I,J are the site indices, $\alpha,\beta \in [d_{xz},d_{yz}]$ are the orbital indices, $s \in [\uparrow,\downarrow]$ is the spin index, and μ is the chemical

potential. $t_{IJ}^{\alpha\beta} \in t_{1-6}$, are the hopping integrals [20,21]. In our previous paper [22] λ_{AOH} could be obtained self-consistently from the nearest-neighbor (NN) interorbital Coulomb interaction at the mean-field level. However, in this paper, we follow the same spirit as Ref. [23] and treat λ_{AOH} and the superconducting pair potential Δ as input parameters for our analysis. The tensor elements $\nu_{I J}^{\alpha\bar{\alpha}} \in [0,\pm 1]$ describe the direction of the NN interorbital currents with $\nu_{\pm\hat{x}}^{12} = \nu_{\pm\hat{y}}^{21} = -1$ and $\nu_{\pm\hat{x}}^{21} = \nu_{\pm\hat{y}}^{12} = 1$. Throughout this paper, all model Hamiltonians (1) and (3) are diagonalized by solving the Bogoliubov–de Gennes (BdG) equations. The chemical potential is adjusted to ensure the system is half filled ($n = 2.0$).

III. EDGE STATES WITH FULLY GAPPED $s_{\pm}$-WAVE PAIRING

The TSC property can be revealed by studying the nature of edge states. We first calculate the energy dispersion under several conditions. Figure 1(a) shows the evolution of the nonsuperconducting (NSC, $\Delta = 0$) band structure with different values of λ_{AOH} in the Brillouin zone (BZ) corresponding to the 2-site per unit cell. In Fig. 1(a), the band crossing below the Fermi energy occurs along the M-Γ direction when there is no existence of anomalous orbital order (AOH), $\lambda_{\text{AOH}} = 0$, and electron and hole pockets are formed at the Fermi energy. In the presence of a small value of the AOH term ($\lambda_{\text{AOH}} = 0.15$), the band crossing is lifted and the four bands are formed into two disentangled groups. However,

the Fermi pockets remain. Furthermore, when the topological order is strong enough [Fig. 1(a) with $\lambda_{\text{AOH}} = 0.6$], an indirect band gap is opened directly at the Fermi energy and the bulk system becomes insulating, from which no superconducting pairing can emerge. Now, we construct a 20×1 lattice strip to study the electronic states at the edge with periodic [for bulk properties; see Figs. 1(b) and 1(d)] and open [for surface properties; see Figs. 1(c) and 1(e)] boundary conditions of the x direction. Since the translational invariance still exists along the strip direction (that is, the y direction) at the original lattice constant, the momentum along this direction is a good quantum number, which allows one to solve the problem for each given wave vector k_y independently. We can see that the edge bands show up by comparing Figs. 1(b) and 1(d) and Figs. 1(c) and 1(e). In the metallic/topological-metallic states ($\lambda_{\text{AOH}} = 0,0.15$) without a superconducting order, the edge bands have curved features across the Fermi surface, as highlighted in red in Fig. 1(c). For $\lambda_{\text{AOH}} = 0$ the nonsuperconducting (NSC) edge states are fourfold degenerate (including two spin orientations and two edges) at a given k_y near the region of $k_y = \pm\frac{\pi}{2}$. When $\lambda_{\text{AOH}} \neq 0$, the degeneracy of edge bands near $k_y = \pm\frac{\pi}{2}$ is reduced to twofold (that is, only twofold spin degeneracy) at a given k_y. However, these bands are still crossing the Fermi energy. We now turn on the $s_{\pm}$-wave pairing ($\Delta = 0.02$) [see Figs. 1(d) and 1(e)]. In the absence of topological order, the edge states have no zero-energy modes, which means the quasiparticle states are always gapped. Only in the presence of a sufficiently large topological order can the edge states appear to cross the Fermi energy [see Fig. 1(e) with $\lambda_{\text{AOH}} = 0.15,0.6$].
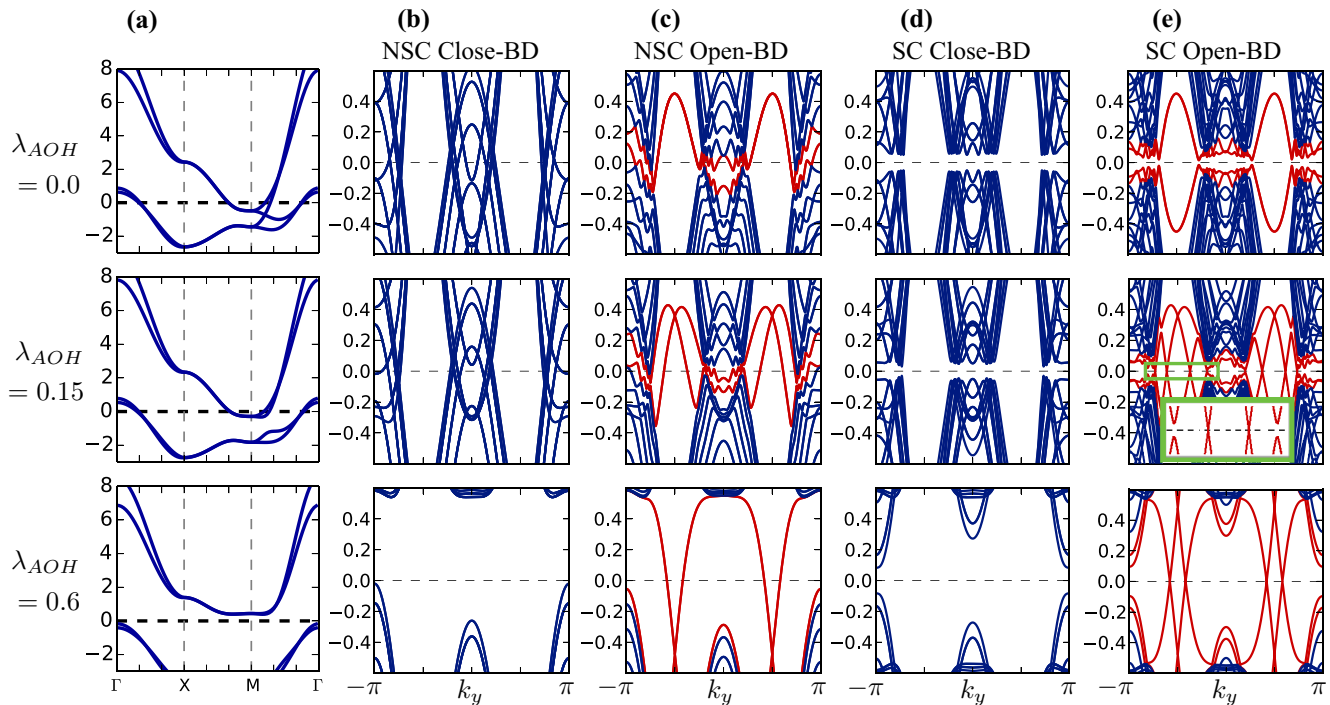

FIG. 1. (Color online) The band structures show the gapless edge states of the coexistence of topological and superconducting orders. (a) The folded band structure of a 2-site per unit cell BZ. (b)–(e) The band structure of a strip of width of 20 lattice constants with open and close boundary conditions under a nonsuperconducting and superconducting phase. We take the periodicity along the y direction of the strip, where 2000 k_y points are taken. The inset of the middle panel of (e) is the enlargement of the crossing point of the Fermi surface, where we can find that there are totally four degenerated points around $k_y = \pm\frac{\pi}{2}$ (the green inset) and the others around $k_y = 0$ and $\pm\pi$ are not degenerated.

We note that for $\lambda_{\mathrm{AOH}} = 0.15$, the normal state is metallic and the superconducting pairing is physically feasible. Therefore, we will focus on the case of $\lambda_{\mathrm{AOH}} = 0.15$ in the next section. For $\lambda_{\mathrm{AOH}} = 0.6$ [see the third row of Fig. 1(e)], the normal state is already insulating and the superconducting pairing is not possible. However, we include this case to show the structure of edge states in response to a "superconducting" particle-particle pair.

IV. LOCAL ELECTRONIC STRUCTURE AROUND AN ADSORBED IMPURITY

The TSC property can also manifest in the local electronic structure around a single impurity. The use of a single impurity is a powerful method to probe the superconducting pairing symmetry [24]. More recently, a universal impurity-induced midgap state has also been predicted as a clear signature of topological superfluids [25,26], where the near-zero-energy bound state closely follows the symmetry of that of Majorana fermions. Inspired by the observation of a robust zero-bias conductance peak in the STM experiments around an interstitial Fe impurity on the surface of the Fe(Te,Se) compound [19], we construct a microscopic model for the local adsorbed impurity within our model. Figure 2(a) shows the 2D lattice structure for a pristine system, where the $d_{xz,yz}$-orbital orientation is considered, while Fig. 2(b) shows an adsorbed Fe atom and its effective local hopping with the neighboring Fe atoms in the parent compound. We write down the total Hamiltonian with the local effect of absorbed impurity site, $\mathcal{H}^{\mathrm{tot}} = \mathcal{H}^{\mathrm{TSC}} + \mathcal{T}^{\mathrm{imp}}[\xi] + \mathcal{S}_z^{\mathrm{imp}}[J]$. $\mathcal{T}^{\mathrm{imp}}$ is the local hopping term from the impurity site to its nearest-neighboring Fe atoms in the parent system with tunable hopping parameter ξ [see Fig. 2(b)], and $\mathcal{S}_z^{\mathrm{imp}}$ describes the local spin-polarized energy

(a)   **(b)**

◆ Up Se/Te   ○ Fe

◆ Dn Se/Te   ╱ dxz orbital   ● IFI $\cdots$ t_σ

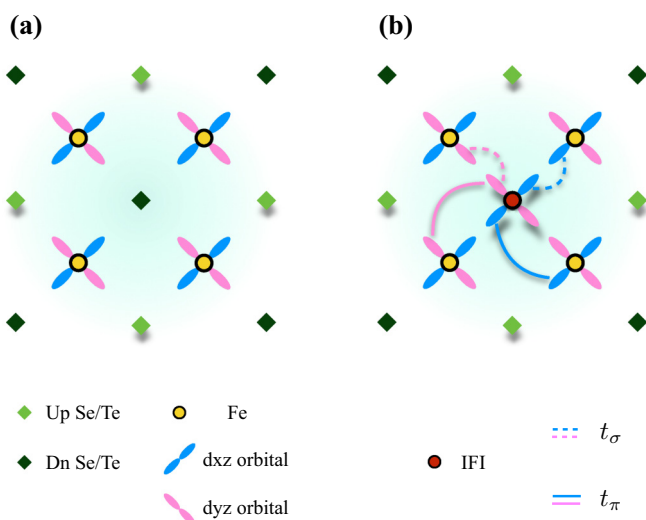   ╲ dyz orbital $=$ t_π

FIG. 2. (Color online) Cartoon picture for an interstitial impurity in a 2D lattice. (a) The top view of the parent lattice structure and the orientation of d_{xz} and d_{yz} orbitals. (b) The position of an interstitial atom located at the center of a plaquette of the 2D square lattice, together with the local hopping process among the d_{xz}/d_{yz} orbitals, where $t_{\sigma,\pi}$ stand for orbital lobes aligned parallel (perpendicular) to the hopping direction between two nearest-neighboring sites of the square lattice. We set $t_\sigma = at_\pi = \xi$ for the parametrization.
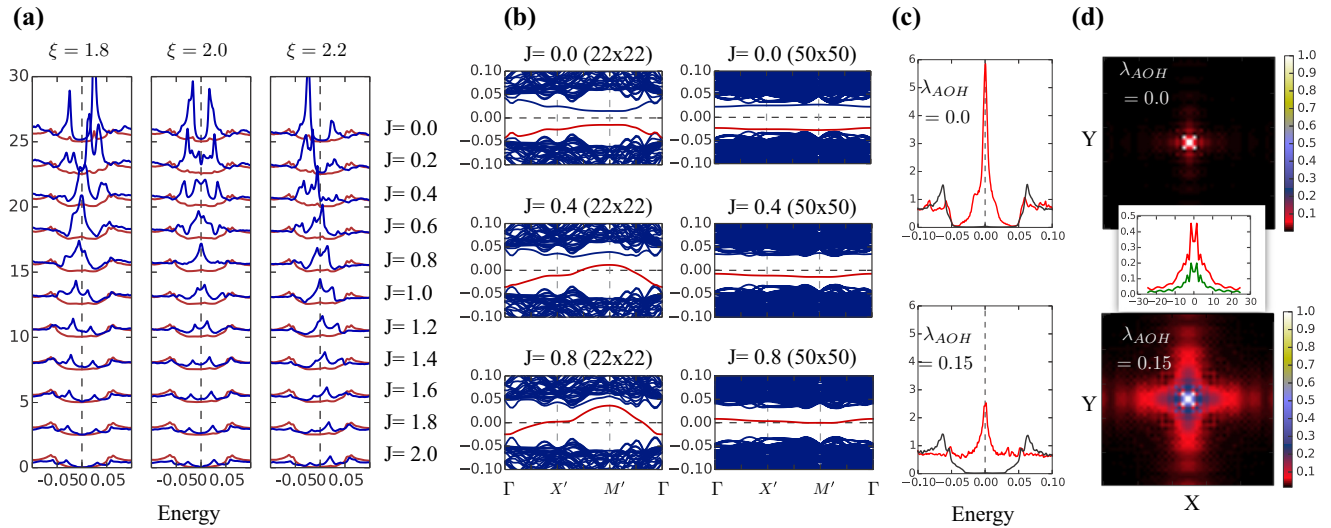
levels on the impurity site with an exchange parameter J, where

$$\mathcal{T}^{\mathrm{imp}} = \sum_{\delta,\alpha,s} t_{\delta\alpha}(c^\dagger_{o,\alpha,s}c_{\delta,\alpha,s} + \mathrm{H.c.}),$$

$$\mathcal{S}_z^{\mathrm{imp}} = (J/2)\sum_{\alpha,ss'} c^\dagger_{o,\alpha,s}(\hat{z}\cdot\vec{\sigma}_{ss'})c_{o,\alpha,s'}. \qquad (3)$$

The index o denotes the impurity site and δ indicates the NN sites from o to its NN sites. $t_{\delta\alpha}$ is the local hopping integral from the impurity site to its NN sites.

We will focus on the local density of states (LDOS) for fixed topological order λ_{AOH} (=0.15 and 0.0) and SC pairing strength Δ (=0.02) with varying ξ and J. Based on the $d_{xz,yz}$-orbital orientation, as shown in Fig. 2(b), there are only two different values in our impurity model $t_{\delta\alpha} \in t_\sigma, t_\pi$; here, we take $t_\sigma = at_\pi = \xi$ with $a = -3$. In our calculation, different signs and magnitudes of a do not change our results qualitatively.

The LDOS can be calculated according to

$$\rho_{i\alpha}(E) = \frac{1}{M}\sum_{n,\mathbf{k}}\left[\left|u^{n,\mathbf{k}}_{i\alpha}\right|^2\delta(E_{n,\mathbf{k}} - E) + \left|v^{n,\mathbf{k}}_{i\alpha}\right|^2\delta(E_{n,\mathbf{k}} + E)\right],$$

$$(4)$$

where the $u^{n,\mathbf{k}}_{i\alpha}$ and $v^{n,\mathbf{k}}_{i\alpha}$ are the eigenfunctions of the BdG matrix of the entire Hamiltonian. We use the broadening facor $\Gamma = 0.001$ in $\delta(x) = \Gamma/\pi(x^2 + \Gamma^2)$. The supercell technique [27] is used for M-repeated cell blocks. In the following section, we numerically solve the band structure of Eq. (1) to reveal the interplay of topological (λ_{AOH}) and superconducting (Δ) orders.

In a regime of weak hybridization, one can anticipate that the resulting peaks in the LDOS on the adsorbed impurity site merely reflect the energy levels of an isolated atom. In our work, we are more interested in the regime where the coupling between the adsorbed impurity and its neighbors is relatively strong. Figure 3(a) shows the LDOS calculated on the adsorbed impurity for various values of ξ and J but with fixed $\Delta = 0.02$ and $\lambda_{\mathrm{AOH}} = 0.15$. For comparison, we also show the LDOS far away from the impurity site [red line in Fig. 3(a)], which resembles the DOS in a pristine bulk. For $J = 0$, since the local hopping is still finite, two in-gap peaks appear near the gap edges. With the increased J, these in-gap peaks are shifted toward the Fermi energy [e.g., in the range of $J \in [0,0.8]$ for $\xi = 2.0$ as shown in Fig. 3(a)], cross the Fermi energy [e.g., at $J \sim 0.8$ for $\xi = 2.0$ as shown in Fig. 3(a)], and move toward the gap edges [e.g., in the range of $J \in [0.8,2.0]$ for $\xi = 2.0$ as shown in Fig. 3(a)]. We also found a regime of $J \in [4,5]$, for which the in-gap quasiparticle peaks show up again. Since in this large J regime the effect of the topological order becomes nonessential, our results are comparable with those in an earlier study on a magnetic impurity in an iron-based superconductor [28]. Therefore, we do not show here the results for this regime. In addition, we note that the in-gap quasiparticle states are of the Shiba nature. The in-gap bound states can also be visualized in the band structure in the reduced Brillouin zone of a supercell lattice [27]. In Fig. 3(b), the band structure is plotted with varying J for fixed values of $\xi = 2$, $\lambda_{\mathrm{AOH}} = 0.15$, and $\Delta = 0.02$. The localization nature of these

FIG. 3. (Color online) LDOS and band dispersion from the model Hamiltonian. (a) The calculated LDOS for various values of spin exchange interaction J on the impurity site (blue lines) and a site deep in the bulk (red lines) as a reference. (b) The highly folded band structure for a supercell (of size $N \times N$) lattice with a single interstitial impurity sitting in the center of each supercell. (c) The LDOS on the interstitial impurity site (red solid lines) and a site deep in the bulk (black solid lines) for $\lambda_{AOH} = 0.0$ (top panel) and $\lambda_{AOH} = 0.15$ (bottom panel) at a fixed $J = 0.8$. (d) The spatial dependence of LDOS at zero energy in the entire supercell of size 50×50. The inset is the cut from site indices $(-24,0)$ to $(25,0)$ along a bond direction through one side of the plaquette in which the interstitial impurity sits [with site coordinate $(0.5,0.5)$]. Unless specified otherwise, the order parameter values are $\lambda_{AOH} = 0.15$ and $\Delta = 0.02$.

in-gap states are investigated by different sizes of the supercell. As shown in Fig. 3(b), the dispersiveness of the in-gap states is suppressed with the increased size of the supercell, suggesting that these in-gap states are truly bound states. We note that the electronic structure shown in Fig. 3(b) arises from the BdG solution with $(u_\uparrow, v_\downarrow)^T$. If we take into account the BdG solution with this $(u_\downarrow, v_\uparrow)^T$, the entire spectrum is symmetric with respect to the Fermi energy. Therefore, we always have a pair of quasiparticle states around the magnetic impurity. This feature is different from the Majorana fermions appearing in a vortex core of exotic superconductors. To further investigate the consequence of the topological order, we show in Fig. 3(c) the LDOS on the impurity site in the absence ($\lambda_{AOH} = 0$) and presence ($\lambda_{AOH} = 0.15$) of topological order. The zero-energy

peak in the LDOS in the absence of topological order is much narrower (accompanied with a higher intensity) than that in the presence of topological order, suggesting a much shorter decay length of the quasiparticle bound state in the former. This contrast is further confirmed by the spatial dependence of the LDOS at zero energy, as shown in Fig. 3(d). Specifically, the zero-energy bound state has a longer decay length along the bond direction in a two-dimensional lattice. This difference can be understood from the band structure of the pristine system in an unfolded Brillouin zone, as shown in Fig. 4, where one can find that the topological order reduces significantly the gap for the wave vector near the X'' point along the Γ-X''-M'' path.

V. RELEVANCE TO RECENT STM EXPERIMENT

We now discuss the relevance of our results to a recent STM experiment on the Fe(Te,Se) compound for an adsorbed Fe impurity [19]. On the one hand, the Fe(Te,Se) compound as mentioned in Ref. [19] has the number of d electrons corresponding to the half filling in the two-orbital model, which is different from highly electron-doped KFe$_2$Se$_2$. Therefore, the chemical potential should be set to ensure the half filling in our calculations. In addition, since the distance from the adsorbed Fe site to its nearest neighbors is shorter than the Fe-Fe bonding distance of the parent compound, we anticipate that the local hopping parameter (ξ) between the adsorbed Fe atom and its neighboring Fe atoms is larger than those for the parent compound. On the other hand, since the superconductivity for iron-based compounds arises from the Fe $3d$ electrons on an essentially square lattice, the normal-state part of the model Hamiltonian originally designed for doped BaFe$_2$As$_2$ [20], to match the low-energy band structure from the local density approximation (LDA)
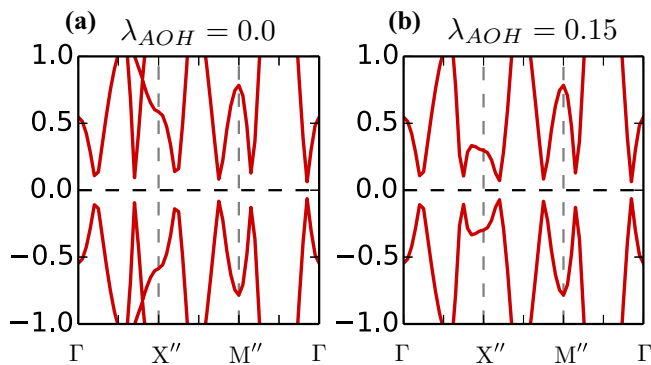

FIG. 4. (Color online) Band structure from the model Hamiltonian. (a) $\lambda_{AOH} = 0$ and (b) $\lambda_{AOH} = 0.15$. The high-symmetry momentum points of Γ, X'', and M'' are defined according to the Brillouin zone of a 1-site per unit cell. The superconducting order parameter $\Delta = 0.02$ is taken.
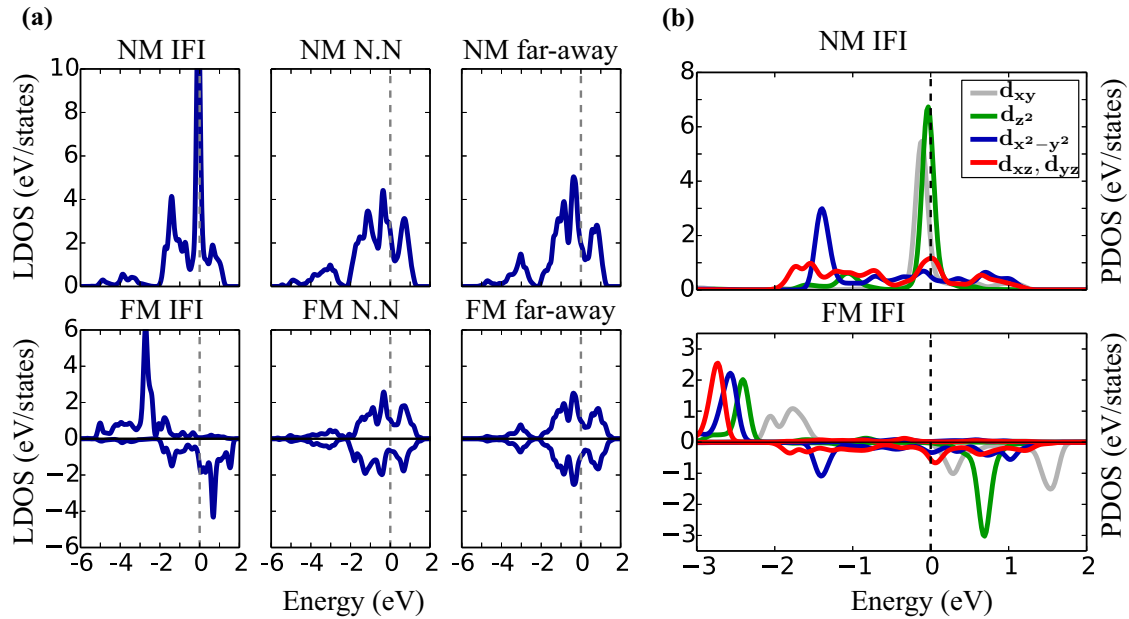
FIG. 5. (Color online) DFT-based local density of states. (a) The local density of states on the IFI, one of its nearest-neighboring Fe sites, far away into pristine FeSe for a nonmagnetic (upper panel) and spin-polarized IFI (lower panel). (b) The d-orbital-resolved partial density of states on the nonmagnetic (upper panel) and spin-polarized (lower panel) IFI site. The positive/negative value of each lower panel describes the up/down spin component.

calculations [29], should also be applicable to the Fe(Te,Se) system.

For the present purpose, we carried out the DFT calculations for an Fe atom adsorbed in the center of Fe plaquette of a large real-space structure of Fe(Te,Se) compound. See the Appendix for the calculation details. We have found that a spin-polarized Fe atom adsorbed on the surface of an otherwise paramagnetic FeSe compound has a lower energy than a non-spin-polarized adsorbed Fe atom. Figure 5(a) shows the calculation of LDOS for both non-spin-polarized (upper panel) and spin-polarized (lower panel) adsorbed Fe atoms. The broadened peak of the LDOS on the adsorbed Fe atom itself and the smearing of the LDOS structure on its neighboring Fe sites in the FeSe compound (as compared with that on the Fe site far way

from the adsorbed Fe atom) suggests a strong coupling between the adsorbed Fe and its neighboring Fe sites. It supports the treatment of the local hopping parameters in our model calculations. For the spin-polarized case, the magnetization is mostly localized on the adsorbed Fe itself with a proximity-induced moment on its nearest-neighboring Fe sites that is negligibly small. Finally, as shown in Fig. 5(b), each d orbital is spin polarized and contributes to the total magnetic moment of $2.89\mu_B$. However, among the total magnetic moments, only about 14.48% (about $0.42\mu_B$) arises from each of the d_{xz} and d_{yz} orbitals, which are relevant to the corresponding orbitals that are active in the pristine compound. These findings support the use of a local magnetic impurity with a small spin polarization in our model calculations.
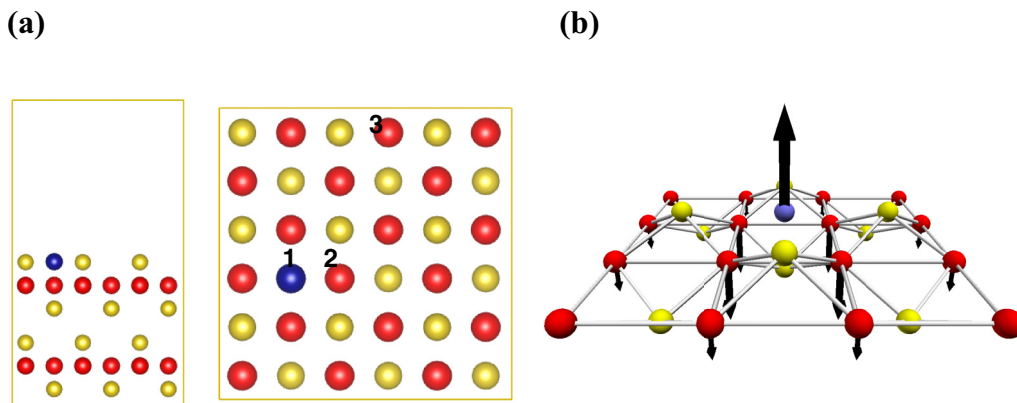

FIG. 6. (Color online) Setup of a two-layered with an adsorbed Fe impurity. (a) The side/top view of the real-space geometry. The labels 1, 2, and 3 indicate the IFI, NN, and far-away sites. (b) Schematic picture showing the DFT calculated magnetic distribution (black arrow). The actual magnitude of each of them is $2.89\mu_B$ (IFI site), $0.23\mu_B$ (NN site), and $0.019\mu_B$ (NNN site). In each panel the red/yellow balls represent Fe/Se atoms while the blue one stands for the IFI.

VI. DISCUSSION

Our model study has shown the combined effect of the Z_2 topological mirror order and the fully gapped $s_\pm$-wave SC. This Z_2 argument extends the mirror symmetry in the mirror Chern representation [16] for the topological superconductivity of a 2D lattice. The coexistence of this topological and superconducting order relies on the intrinsic band structure of the $d_{xz,yz}$ orbitals, which gives a topological metallic state. There, the emergence of gapless edge states in the coexisting phase is direct evidence of the topological order. In addition, the introduction of a spin-polarized impurity can be regarded as a zero-dimension boundary to the 2D lattice, and it induces a similar quasiparticle behavior as around a vortex core center in the topological superconductor [30]. In addition, our model calculations of the local electronic structure have revealed the topological feature of a superconductor through the LDOS peak intensity and the size of the impurity-induced in-gap bound states. Finally, our DFT calculations of an adsorbed Fe atom on the surface of the FeSe compound have indeed shown the adsorbed impurity is spin polarized, making the findings in the present work relevant to the STM experiment on the Fe(Te,Se) compound.

Note added. Recently, we became aware of a study by Zhang [31] that described the in-gap bound state around an adsorbed Fe atom on the surface of iron-based superconductors, within an impurity model with non-spin-polarized d electrons on the impurity site. Due to the mismatch of energy levels between the impurity and the Fe sites in the background, the qualitative agreement with the STM experiment [19] was obtained by adjusting the chemical potential in the pristine system under the strict condition of a relatively small hybridization between the adsorbed Fe atom and its neighbors. The shifted chemical potential leads to the system in the highly electron doped regime, which appears inconsistent with the fact that Fe(Se,Te) is in the half-filled regime in the two-orbital model. In addition, it can be understood that with a small hybridization, the zero-energy peak at the adsorbed Fe site has the character of the energy levels of an isolated atom so that the peak intensity is high.

APPENDIX: DFT CALCULATION METHODS

We use the Vienna *ab initio* simulation package (VASP) [32] to carry out the LDA calculations for an interstitial Fe impurity (IFI) atom sitting in the center of a large real-space structure of a Fe(Te,Se) compound. The projector augmented plane-wave method [33] and the Perdew-Burke-Ernzerhof [34] exchange-correlation functional were adopted. We used a $4 \times 4 \times 2$ Monkhorst-Pack k-point mesh, and a 500 eV cutoff. The z coordinate of Fe impurity atoms was fully relaxed up to 10^{-2} eV/Å with other atoms fixed.

We have considered the setup as shown in Fig. 6(a), in which an IFI atom sits on top of a two-layered FeSe. A vacancy space in the z direction was made to mimic the surface effect of the single IFI atom. We have calculated (i) a nonmagnetic (NM) state and (ii) a ferromagnetic (FM) state on the IFI site by turning the spin polarization on and off initially on the IFI site. Each of the two calculations has reached the charge convergence. Figure 6(b) shows the local distribution of the magnetic moment. The calculated total energy shows that case (ii) is more stable than case (i), which confirms a spin-polarized IFI site.

[1] A. Y. Kitaev, Phys.-Usp. **44**, 131 (2001).

[2] J. Linder and J. W. A. Robinson, Nat. Phys. **11**, 307 (2015).

[3] L. Fu and C. L. Kane, Phys. Rev. Lett. **100**, 096407 (2008).

[4] I. Martin and A. F. Morpurgo, Phys. Rev. B **85**, 144505 (2012).

[5] M. M. Vazifeh and M. Franz, Phys. Rev. Lett. **111**, 206802 (2013).

[6] F. Pientka, L. I. Glazman, and F. von Oppen, Phys. Rev. B **88**, 155420 (2013).

[7] J. Klinovaja, P. Stano, A. Yazdani, and D. Loss, Phys. Rev. Lett. **111**, 186805 (2013).

[8] I. Reis, D. J. J. Marchand, and M. Franz, Phys. Rev. B **90**, 085124 (2014).

[9] S. Nadj-Perge, I. K. Drozdov, J. Li, H. Chen, S. Jeon, J. Seo, A. H. MacDonald, B. A. Bernevig, and A. Yazdani, Science **346**, 602 (2014).

[10] J. Li, H. Chen, I. K. Drozdov, A. Yazdani, B. A. Bernevig, and A. H. MacDonald, Phys. Rev. B **90**, 235433 (2014).

[11] P. M. R. Brydon, S. Das Sarma, H.-Y. Hui, and J. D. Sau, Phys. Rev. B **91**, 064505 (2015).

[12] A. Heimes, D. Mendler, and P. Kotetes, New J. Phys. **17**, 023051 (2015).

[13] Y. Peng, F. Pientka, L. I. Glazman, and F. von Oppen, Phys. Rev. Lett. **114**, 106801 (2015).

[14] J. Zhang, Y. Kim, E. Rossi, and R. M. Lutchyn, arXiv:1505.05862.

[15] X.-L. Qi, T. L. Hughes, and S.-C. Zhang, Phys. Rev. B **82**, 184516 (2010).

[16] F. Zhang, C. L. Kane, and E. J. Mele, Phys. Rev. Lett. **111**, 056403 (2013).

[17] X.-L. Qi, T. L. Hughes, S. Raghu, and S.-C. Zhang, Phys. Rev. Lett. **102**, 187001 (2009).

[18] Y. Ueno, A. Yamakage, Y. Tanaka, and M. Sato, Phys. Rev. Lett. **111**, 087002 (2013).

[19] J.-X. Yin, Zheng Wu, J.-H. Wang, Z.-Y. Ye, Jing Gong, X.-Y. Hou, Lei Shan, Ang Li, X.-J. Liang, X.-X. Wu, Jian Li, C.-S. Ting, Z.-Q. Wang, J.-P. Hu, P.-H. Hor, H. Ding, and S. H. Pan, Nat. Phys. **11**, 543 (2015).

[20] Y.-Y. Tai, J.-X. Zhu, M. J. Graf, and C. S. Ting, Europhys. Lett. **103**, 67001 (2013).

[21] H. Chen, Y.-Y. Tai, C. S. Ting, M. J. Graf, J. Dai, and J.-X. Zhu, Phys. Rev. B **88**, 184509 (2013).

[22] Y.-Y. Tai, C.-C. J. Wang, M. J. Graf, J.-X. Zhu, and C. S. Ting, Phys. Rev. B **91**, 041111(R) (2015).

[23] J.-X. Zhu, I. Martin, and A. R. Bishop, Phys. Rev. Lett. **100**, 236403 (2008).

[24] A. V. Balatsky, I. Vekhter, and J.-X. Zhu, Rev. Mod. Phys. **78**, 373 (2006).

[25] X.-J. Liu and H. Hu, Phys. Rev. A **85**, 033622 (2012).

[26] H. Hu, L. Jiang, H. Pu, Y. Chen, and X.-J. Liu, Phys. Rev. Lett. **110**, 020401 (2013).

[27] J.-X. Zhu, B. Friedman, and C. S. Ting, Phys. Rev. B **59**, 3353 (1999).

[28] W.-F. Tsai, Y.-Y. Zhang, C. Fang, and J. Hu, Phys. Rev. B **80**, 064513 (2009).

[29] A. Subedi, L. Zhang, D. J. Singh, and M. H. Du, Phys. Rev. B **78**, 134514 (2008).

[30] M. Sato and S. Fujimoto, Phys. Rev. B **79**, 094504 (2009).

[31] D. Zhang, Physica C **519**, 43 (2015).

[32] G. Kresse and J. Furthmüller, Phys. Rev. B **54**, 11169 (1996).

[33] G. Kresse and D. Joubert, Phys. Rev. B **59**, 1758 (1999).

[34] J. P. Perdew, K. Burke, and M. Ernzerhof, Phys. Rev. Lett. **77**, 3865 (1996).